Terahertz intersubband absorption in GaN/AlGaN step quantum wells

H. Machhadani,[1] Y. Kotsar,[2] S. Sakr,[1] M. Tchernycheva,[1] R. Colombelli,[1] J. Mangeney,[1] E. Bellet-Amalric,[2] E. Sarigiannidou,[3] E. Monroy,[2] and F. H. Julien[1,a)]
[1]*Institut d'Electronique Fondamentale, University Paris-Sud 11, UMR 8622 CNRS, 91405 Orsay Cedex, France*
[2]*CEA-CNRS Group "Nanophysique et Semiconducteurs," INAC/SP2M/NPSC, CEA-Grenoble, 17 rue des Martyrs, 38054 Grenoble Cedex 9, France*
[3]*LMGP/LTM, Grenoble INP, 3 Parvis Louis Néel, 38016 Grenoble Cedex 1, France*

(Received 15 October 2010; accepted 22 October 2010; published online 8 November 2010)

We demonstrate terahertz intersubband absorptions at frequencies of 2.1 THz ($\lambda \approx 143$ μm) and 4.2 THz ($\lambda \approx 70$ μm) in nitride-based semiconductor quantum wells. The structures consist of a 3 nm thick GaN well, an $Al_{0.05}Ga_{0.95}N$ step barrier, and a 3 nm thick $Al_{0.1}Ga_{0.9}N$ barrier. The absorption is detected at 4.7 K. The structure design has been optimized to approach a flat-band potential in the wells to allow for an intersubband absorption in the terahertz frequency range and to maximize the optical dipole moments. © *2010 American Institute of Physics*. [doi:10.1063/1.3515423]

The terahertz spectral region is subject to intensive research in view of its potential in a number of application domains such as medical diagnostics, security screening, or quality control. In terms of sources, quantum cascade lasers (QCLs) based on intersubband (ISB) transitions in GaAs/AlGaAs quantum wells (QWs) have emerged as excellent candidates for applications requiring a few tens-of-milliwatt power in the 1.2–5 THz spectral range.[1–4] Although much progress has been accomplished in terms of performance, including high-brightness terahertz QCL,[5] the maximum operating temperatures reported so far—186 and 120 K for pulsed and continuous wave operation—are still too low for widespread applications.[6,2(a)] One intrinsic reason limiting the temperature is the small energy of the longitudinal optical (LO) phonon in GaAs (36 meV, 8.2 THz), which hinders laser action close to room temperature because of thermally activated LO-phonon emission. It was predicted that wide band gap semiconductor materials such as GaN, with a LO-phonon energy of 92 meV (22.3 THz), pave the way for terahertz QCLs operating above room temperature.[7–9] In addition, GaN QCLs could operate at frequencies out of range of GaAs QCLs, i.e., 4.6–12 THz corresponding to the reststrahlen absorption of GaAs.

So far, most of the research on GaN-based ISB transitions has focused on near-infrared applications, benefiting from the large conduction-band offset between GaN and AlN (1.75 eV).[10] Devices such as all-optical switches, electro-optical modulators, quantum cascade detectors, or light emitters have been demonstrated at short infrared wavelengths.[11–15] It was shown that the ISB absorption wavelength can be tuned up to the Reststrahlen band of GaN (12–20 μm, 15–25 THz) by reducing the internal field inherent to polar GaN grown along the c-axis.[16] This can be achieved by reducing the Al content of the barriers, increasing the well thickness and decreasing the barrier thickness.[17] Although efficient in the midinfrared spectral range, this strategy is expected to raise difficulties at longer wavelengths because of the blue-shift induced by many-body effects arising from the intentional or nonintentional doping of the quantum wells.[18]

In this paper, we demonstrate an alternative strategy aimed at achieving terahertz ISB absorption in GaN QWs. The core idea is to approach a flat potential in the QW layers by engineering the internal electric field. The structures under investigation are superlattices of step-QWs, composed of a GaN well, an $Al_{0.05}Ga_{0.95}N$ step barrier, and an $Al_{0.1}Ga_{0.9}N$ barrier. Measurements performed at 4 K reveal transverse-magnetic (TM) polarized ISB absorption at 4.2 and 2.1 THz, respectively, in good agreement with simulations.

The sample active region consists of a superlattice of step-QWs formed by an $Al_{0.05}Ga_{0.95}N$ step barrier, a 3 nm thick GaN well, and a 3 nm thick $Al_{0.1}Ga_{0.9}N$ spacer barrier. The step barrier thickness is 10 nm (15 nm) for sample A (B). The GaN wells are n-doped with silicon at a nominal concentration of 1×10^{19} cm^{-3} (5×10^{18} cm^{-3}) for sample A (B). Figures 1(a) and 1(b) show the conduction-band profile and squared envelope functions for samples A and B, respectively. Calculations were performed using a self-consistent Schrödinger–Poisson solver accounting for conduction-band nonparabolicity using the material parameters described in Ref. 10 and assuming periodic potential conditions.[17] The bowing parameter of the AlGaN band gap was taken as 1 eV. As seen in Fig. 1, the potential in the step barrier is almost flat except for a slight band bending due to the Coulomb interaction between electrons and ionized donors. The ground and excited electronic states are confined in the GaN well and $Al_{0.05}Ga_{0.95}N$ step barrier. This leads to a large ISB dipole length of 2.76 (3.84) nm for sample A (B). The e_1e_2 ISB transition energy is predicted at 21 meV (10 meV) for sample A (B). This corresponds to 5.1 and 2.4 THz, respectively.

The samples consist of 40 QW repetitions based on the above-described designs. They were grown by plasma-assisted molecular beam epitaxy on a commercial crack-free GaN high electron mobility transistor structure grown on Si(111) [referred hereafter as GaN-on-Si(111) template]. The active region was sandwiched between two 50-nm-thick $Al_{0.05}Ga_{0.95}N$ unintentionally doped cladding layers. The whole structure was grown at a substrate temperature of 720 °C under Ga-rich conditions and without growth inter-

a)Author to whom correspondence should be addressed. Electronic mail: francois.julien@u-psud.fr.

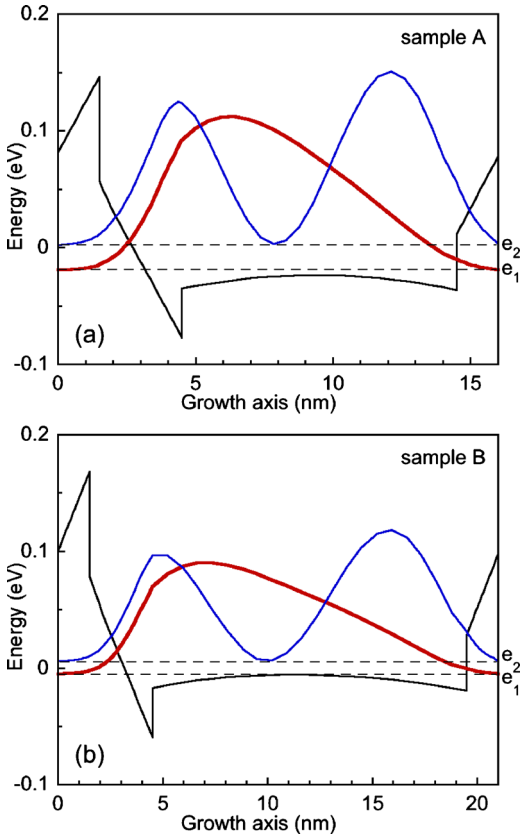

FIG. 1. (Color online) Conduction-band profile and squared envelope functions of first two electronic levels (e_1, e_2) for (a) sample A with 10 nm thick step barrier and (b) sample B with 15 nm thick step barrier.

ruptions. The various layer thicknesses were verified by cross-section conventional transmission electron microscopy, as illustrated for sample A in the micrograph in Fig. 2. The image contrast qualitatively correlates with the chemical composition of the layers. High-resolution transmission electron microscopy shows no indication of stacking faults or extended defects in the active region. Additional structural characterization by high-resolution x-ray diffraction (see Fig. 2) points to a period about 6% smaller than the nominal value in both samples, with Al mole fractions that could also be slightly smaller (by ~10%) than the nominal value.[19]

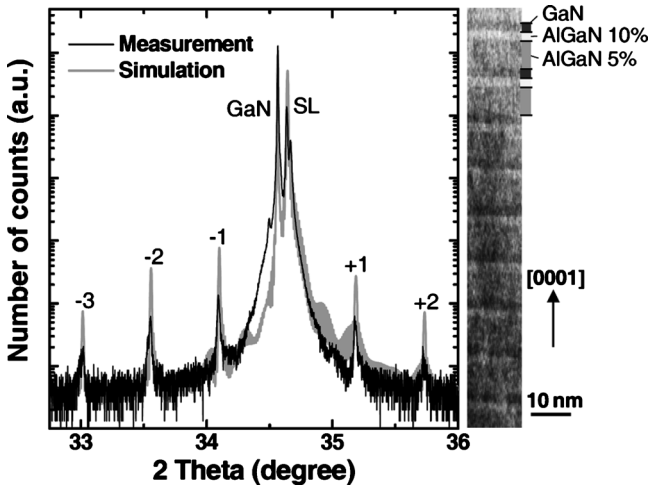

FIG. 2. High-resolution $\omega-2\theta$ scan around the (0002) x-ray reflection of sample A compared to a theoretical calculation using the X'PERT EPITAXY 40 software from Phillips Analytical (SL=superlattice reflection). On the right is the cross-section conventional transmission electron microscopy image of the active region of sample A, where the image contrast correlates with the chemical composition of the layers.

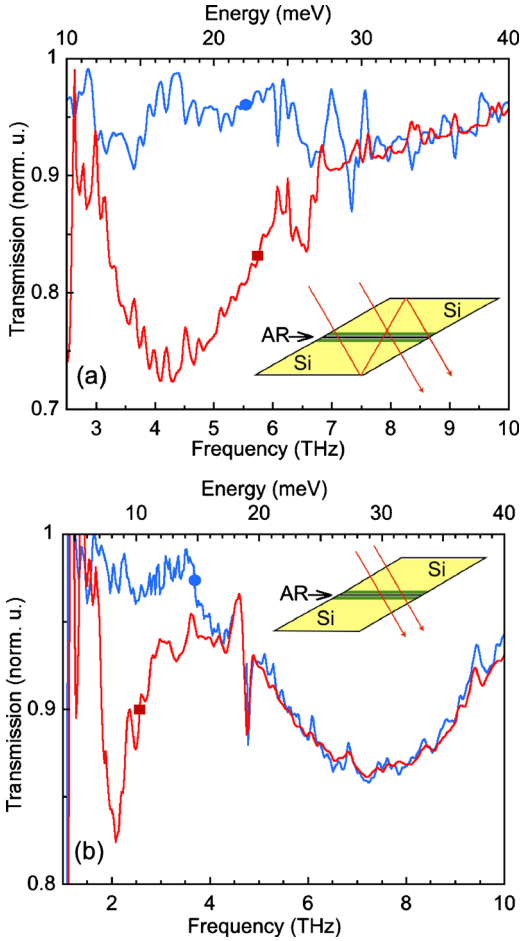

FIG. 3. (Color online) Transmission spectra for TM- (square) and TE-polarized (circle) light at 4.7 K for samples A (a) and B (b). The insets show the experimental configuration with two pieces face-to-face and the ray tracing. The active regions (AR) are shown by an arrow.

For transmission measurements, the samples were diced in two pieces of equal length (3.9 and 3.51 mm for samples A and B, respectively). The thickness of each piece was 0.62 (0.61) mm for sample A (B). We then mechanically polished the two opposite facets of each piece at an angle of 30°. This angle was chosen to avoid total internal reflection at the interface between the high index-of-refraction silicon substrate and the active region when illuminating the input facet at normal incidence. The two pieces were placed face-to-face under mechanical pressure on the cold finger of a liquid helium-cooled cryostat. This configuration provides a good coupling of the TM-polarized terahertz radiation with the ISB transitions and it allows an enhancement of the ISB absorption by doubling the number of periods. The transmission measurements were performed at 4.7 K using a Bruker Fourier transform infrared spectrometer equipped with a glow-bar source. Detection was provided by a liquid helium-cooled Si bolometer. Two pieces of GaN-on-Si(111) templates placed face-to-face were used as a reference. Each piece had a length of 3.6 mm and a thickness of 0.55 mm.

Figures 3(a) and 3(b) show the transmission spectrum of samples A and B, respectively, for TM- and TE-polarized light. The transmission of the samples divided by the trans-

mission of the reference sample has been normalized to 1 at low frequencies. As seen in Fig. 3, samples A and B exhibit an absorption peaked at 4.2 THz (17.4 meV) and 2.1 THz (8.7 meV), respectively, only for TM-polarized light. This is a clear indication of the ISB origin of the observed absorption. The baseline for TE-polarized light is not flat possibly because of the slightly different length and thickness of the reference and active samples. The peak ISB absorption energy of both samples is in good agreement with simulations using the nominal growth parameters. The full width at half maximum (FWHM) of the TM-polarized absorption is 2.4 THz for sample A and 0.72 THz for sample B, which values correspond to a broadening factor $(\Delta\lambda/\lambda)$ of 54% and 34% for samples A and B, respectively. Simulations show that this rather large broadening cannot be attributed to the fluctuations of the layer thickness. Indeed, assuming a ± 1 ML thickness variation of the well and of the step and separating barriers, the relative shift of the ISB wavelength is calculated to be $\Delta\lambda/\lambda = 14\%$ (8%) for sample A (B). We believe that the main contributions to the broadening are the electron-impurity and electron-electron scatterings, based on the fact that the FWHM of the lower doped sample B is smaller than that of sample A.

We now describe the procedure to estimate the electron concentration in the wells.[20] The peak absorbance deduced from the transmission measurements of Fig. 3 is ~0.33 (0.2) for sample A (B). The effective number of passes through the active layers is calculated to be 1.5 (1) for sample A (B), as illustrated in the insets of Fig. 3. Based on the calculated dipole length and on the experimental transition energy and broadening, the absorption cross-section is estimated to be 1.6×10^{-15} cm^{-2} (5.5×10^{-15} cm^{-2}) for sample A (B) accounting for a 52° refraction angle in the active layers. For sample A, the surface electron density difference between the e_1 and e_2 subbands is deduced to be $n_1-n_2\sim1.6\times10^{12}$ cm^{-2}, which corresponds to a Fermi energy E_f above the e_2 state. This experimental value is in excellent agreement with the theoretical estimate assuming $E_f-e_2>$kT,

$$n_1 - n_2 \approx \frac{m^* E_{21}}{\pi\hbar^2},$$

where kT is the thermal energy, m^* the effective mass, E_{21} the ISB transition energy, and $\hbar$ the reduced Planck constant. For sample B, the surface electron density is deduced to be 4.5×10^{11} cm^{-2} and the Fermi energy is 5 meV above the e_1 state, which means that only the ground state is significantly populated at 4.7 K. The deduced volumic electron concentration is smaller by a factor of about 3 than the value deduced from the nominal doping concentration, which may be attributed to a partial ionization of the silicon impurities in GaN at 4.7 K.

In conclusion, we have reported the observation of ISB absorption at terahertz frequencies in GaN/AlGaN step-QWs. The absorption peaks are at frequencies of 4.2 and 2.1 THz, respectively. The sample design targets a flat-band potential in the wells to allow for an ISB absorption in the terahertz frequency range and to improve the optical dipole moments. The rather large broadening of the ISB absorption (in the range of 34%–54%) is attributed to electron-impurity and electron-electron scattering due to the large doping and carrier concentration.

The authors acknowledge the fruitful discussions with Y. Todorov as well as the financial support of EC FET-OPEN program "Unitride" under Grant Agreement No. 233950. The GaN-on-Si(111) structures used as substrates were provided by DOWA Electronics Materials.

[1] R. Köhler, A. Tredicucci, F. Beltram, H. E. Beere, E. H. Linfield, A. G. Davies, D. A. Ritchie, R. C. Iotti, and F. Rossi, Nature (London) **417**, 156 (2002).
[2] (a) B. S. Williams, S. Kumar, Q. Hu, and J. L. Reno, Opt. Express **13**, 3331 (2005); (b) B. S. Williams, S. Kumar, Q. Qin, Q. Hu, and J. L. Reno, Appl. Phys. Lett. **88**, 261101 (2006).
[3] C. Walther, M. Fischer, G. Scalari, R. Terazzi, N. Hoyler, and J. Faist, Appl. Phys. Lett. **91**, 131122 (2007).
[4] H. Luo, S. R. Laframboise, Z. R. Wasilewski, G. C. Aers, H. C. Liu, and J. C. Cao, Appl. Phys. Lett. **90**, 041112 (2007).
[5] Y. Chassagneux, R. Colombelli, W. Maineult, S. Barbieri, H. E. Beere, D. A. Ritchie, S. P. Khanna, E. H. Linfield, and A. G. Davies, Nature (London) **457**, 174 (2009).
[6] S. Kumar, Q. Hu, and J. L. Reno, Appl. Phys. Lett. **94**, 131105 (2009).
[7] V. D. Jovanović, D. Indjin, Z. Ikonić, and P. Harrison, Appl. Phys. Lett. **84**, 2995 (2004).
[8] E. Bellotti, K. Driscoll, T. D. Moustatkas, and R. Paiella, Appl. Phys. Lett. **92**, 101112 (2008).
[9] E. Bellotti, K. Driscoll, T. D. Moustatkas, and R. Paiella, J. Appl. Phys. **105**, 113103 (2009).
[10] M. Tchernycheva, L. Nevou, L. Doyennette, F. H. Julien, E. Warde, F. Guillot, E. Monroy, E. Bellet-Amalric, T. Remmele, and M. Albrecht, Phys. Rev. B **73**, 125347 (2006).
[11] N. Iizuka, K. Kaneko, and N. Suzuki, Opt. Express **13**, 3835 (2005).
[12] L. Nevou, N. Kheirodin, M. Tchernycheva, L. Meignien, P. Crozat, A. Lupu, E. Warde, F. H. Julien, G. Pozzovivo, S. Golka, G. Strasser, F. Guillot, E. Monroy, T. Remmele, and M. Albrecht, Appl. Phys. Lett. **90**, 223511 (2007).
[13] A. Vardi, N. Kheirodin, L. Nevou, H. Machhadani, L. Vivien, P. Crozat, M. Tchernycheva, R. Colombelli, F. Julien, F. Guillot, C. Bougerol, E. Monroy, S. Schacham, and G. Bahir, Appl. Phys. Lett. **93**, 193509 (2008).
[14] L. Nevou, M. Tchernycheva, F. H. Julien, F. Guillot, and E. Monroy, Appl. Phys. Lett. **90**, 121106 (2007).
[15] K. Driscoll, A. Bhattacharyya, L. Zhou, D. J. Smith, T. D. Moustakas, and R. Paiella, Appl. Phys. Lett. **94**, 081120 (2009).
[16] P. K. Kandaswamy, H. Machhadani, C. Bougerol, F. H. Julien, and E. Monroy, Appl. Phys. Lett. **95**, 141911 (2009).
[17] H. Machhadani, P. Kandaswamy, S. Sakr, A. Vardi, A. Wirtmüller, L. Nevou, F. Guillot, G. Pozzovivo, M. Tchernycheva, A. Lupu, L. Vivien, P. Crozat, E. Warde, C. Bougerol, S. Schacham, G. Strasser, G. Bahir, E. Monroy, and F. H. Julien, New J. Phys. **11**, 125023 (2009).
[18] P. K. Kandaswamy, H. Machhadani, Y. Kotsar, S. Sakr, A. Das, M. Tchernycheva, L. Rapenne, E. Sarigiannidou, F. H. Julien, and E. Monroy, Appl. Phys. Lett. **96**, 141903 (2010).
[19] Due to the complexity of the buffer structure of the GaN-on-Si(111) templates, x-ray diffraction analysis was performed on samples grown simultaneously on GaN-on-sapphire templates.
[20] M. Helm, in *Intersubband Transitions in Quantum Wells: Physics and Device Applications I*, edited by H. C. Liu and F. Capasso (Academic, New York, 2000).